Published in final edited form as:
Acta Biomater. 2010 October ; 6(10): 4118–4126. doi:10.1016/j.actbio.2010.04.029.

Human bone marrow stem cell-encapsulating calcium phosphate scaffolds for bone repair

Michael D. Weir[a] and **Hockin H.K. Xu**[a,b,c,*]

[a]Department of Endodontics, Prosthodontics and Operative Dentistry, University of Maryland Dental School, Baltimore, MD 21201, USA

[b]Center for Stem Cell Biology and Regenerative Medicine, University of Maryland School of Medicine, Baltimore, MD 21201, USA

[c]Department of Mechanical Engineering, University of Maryland, Baltimore County, MD 21250, USA

Abstract

Due to its injectability and excellent osteoconductivity, calcium phosphate cement (CPC) is highly promising for orthopedic applications. However, a literature search revealed no report on human bone marrow mesenchymal stem cell (hBMSC) encapsulation in CPC for bone tissue engineering. The aim of this study was to encapsulate hBMSCs in alginate hydrogel beads and then incorporate them into CPC, CPC–chitosan and CPC–chitosan–fiber scaffolds. Chitosan and degradable fibers were used to mechanically reinforce the scaffolds. After 21 days, that the percentage of live cells and the cell density of hBMSCs inside CPC-based constructs matched those in alginate without CPC, indicating that the CPC setting reaction did not harm the hBMSCs. Alkaline phosphate activity increased by 8-fold after 14 days. Mineral staining, scanning electron microscopy and X-ray diffraction confirmed that apatitic mineral was deposited by the cells. The amount of hBMSC-synthesized mineral in CPC–chitosan–fiber matched that in CPC without chitosan and fibers. Hence, adding chitosan and fibers, which reinforced the CPC, did not compromise hBMSC osteodifferentiation and mineral synthesis. In conclusion, hBMSCs were encapsulated in CPC and CPC–chitosan–fiber scaffolds for the first time. The encapsulated cells remained viable, osteodifferentiated and synthesized bone minerals. These self-setting, hBMSC-encapsulating CPC-based constructs may be promising for bone tissue engineering applications.

Keywords

Stem cell encapsulation; Osteogenic differentiation; Alginate hydrogel; Calcium phosphate cement scaffold; Bone marrow mesenchymal stem cells

1. Introduction

Bone tissue reconstruction frequently arises from skeletal diseases, congenital malformations, infection, trauma and post-cancer ablative surgery [1]. Autologous and allogenic bone grafts currently comprise about 90% of grafts performed each year, with synthetic grafts comprising the remaining 10% [2]. Recent work has sought to combine

*Corresponding author at: Department of Endodontics, Prosthodontics and Operative Dentistry, University of Maryland Dental School, Baltimore, MD 21201, USA. Tel.: +1 410 706 7047; fax: +1 410 706 3028. hxu@umaryland.edu, Uhxu@umaryland.edu (H.H.K. Xu).

biomaterial scaffolds and cells to create synthetic matrices for tissue regeneration that match the physical and biological properties of natural tissue. Stem cells in particular have drawn interest because they are undifferentiated cells with the ability to differentiate into one or more types of cells and are capable of self-renewal [3,4]. Human bone marrow-derived mesenchymal stem cells (hBMSCs) have the ability to differentiate into osteoblasts, adipocytes, chondrocytes, myoblasts, cardiomyocytes, hepatocytes, neurons, astrocytes, endothelial cells, fibroblasts and stromal cells [3]. hBMSCs are easily accessible, have the capacity for expansion and possess minimal immunogenic and tumorigenic hazards. Because of these factors, hBMSCs are thought to be an excellent cell source for dental, craniofacial and orthopedic repairs.

The combination of hBMSCs and bioengineered scaffolds for bone regeneration has been investigated by many research groups. Investigators have encapsulate stem cells in hydrogels such as alginate [5,6], hyaluronic acid [7] and those based on poly(ethylene glycol) [8–10] for cartilage tissue engineering applications. However, these hydrogels do not provide the strength necessary for bone repair in load-bearing locations. For bone tissue engineering applications, where enhanced mechanical properties are desirable, materials such as collagen, chitosan, polycaprolactone, polyanhydrides and poly(D,L-lactide-co-glycolide) have been developed [11]. Likewise, inorganic scaffolds consisting of calcium phosphate bioceramics have also been used for bone repair [12–14]. These are pre-formed implants that are not injectable. Another inorganic material, hydroxyapatite, has been used as a matrix for hard tissue repair because of its similarity to the minerals in bone [15–18]. Although sintered hydroxyapatite is mechanically stronger, it has to be shaped ex vivo, may not fit intimately into the bone cavity and is not resorbable.

There are several calcium phosphate cements that are injectable and can self-harden in situ to form bioresorbable hydroxyapatite in the bone cavity [19–24]. The first calcium phosphate cement was developed by Brown and Chow in 1986; it was referred to as CPC and consisted of a mixture of tetracalcium phosphate and anhydrous dicalcium phosphate [22]. CPC paste can fill a bone defect with an intimate adaptation to complex cavities. Once hardened, a resorbable and microcrystalline hydroxyapatite is formed [25,26]. The moldability, biocompatibility, osteoconductivity and resorbability make CPC an excellent candidate for maxillofacial and orthopedic applications. As a result, CPC was approved in 1996 by the Food and Drug Administration (FDA) for repairing craniofacial defects in humans (BoneSource, Orthofix/OsteoGenics, Richardson, TX), thus becoming the first CPC approved for clinical use [27]. However, the poor mechanical properties of this CPC have limited its use to primarily low stress-bearing applications [28]. Methods to improved the mechanical properties of CPC have included the addition of degradable poly(lactide-co-glycolide) fibers to the CPC paste [29]. Over time degradation of the fibers could coincide with the ingrowth of new bone. The addition of chitosan lactate and reinforcing fibers had a synergistic effect in enhancing the physical properties of CPC for bone tissue engineering.

When cultured with preosteoblast cells, CPC and CPC–chitosan scaffolds were shown to be non-cytotoxic and supported cell growth and proliferation [30]. However, recent work has indicated that pH changes and ionic activity in the CPC setting reaction may have an adverse effect on hBMSCs seeded directly on the surface of CPC, without encapsulation of the hBMSCs inside the CPC paste [31].

Therefore, the objectives of the present study were to: (1) encapsulate hBMSCs into alginate hydrogel beads and then incorporate them into high strength CPC–chitosan and CPC–chitosan– fiber scaffolds; (2) induce the encapsulated hBMSCs to differentiate down the osteogenic lineage. The hypotheses were: (1) encapsulating hBMSCs in an alginate hydrogel will protect the hBMSCs during the CPC setting reaction; (2) the hBMSCs can undergo

osteogenic differentiation, with elevated alkaline phosphatase (ALP) activity and mineralization, while encapsulated in the CPC-based constructs.

2. Materials and methods

2.1. CPC powder and liquid

The CPC powder consisted of an equimolar mixture of tetracalcium phosphate (TTCP) ($Ca_4[PO_4]_2O$) and anhydrous dicalcium phosphate (DCPA) ($CaHPO_4$), which was prepared according to a previous study [32]. The CPC liquid consisted of chitosan lactate (Halosource Inc., Redmond WA), referred to as chitosan, mixed with distilled water at a chitosan/(chitosan + water) mass fraction of 15%. The purpose of adding chitosan to CPC was to make it faster setting and stronger [29]. Traditional CPC, using water as the liquid component, was used as a control. A powder to liquid mass ratio of 3:1 was used. A degradable suture fiber (Vicryl, Ethicon, Somerville, NJ), which is a co-polymer of glycolic and lactic acids, was cut into 8 mm long filaments and used to reinforce the CPC–cell construct, because of its relatively high strength [33]. This suture consisted of fibers braided into a bundle with a diameter of approximately 322 μm (from the manufacturer's specifications), suitable for creating macropore channels after fiber dissolution. The CPC powder, chitosan lactate powder and the pre-cut Vicryl fibers were sterilized in an ethylene oxide sterilizer (Anprolene AN 74i, Andersen, Haw River, NC) for 12 h according to the manufacturer's specifications. After sterilization the materials were degassed for a minimum of 72 h under vacuum.

2.2. hBMSC culture and encapsulation

hBMSCs (Poietics, Lonza, Allendale, NJ) were cultured following established protocols [34] at 37 °C with 5% CO_2 in low glucose Dulbecco's modified Eagle's medium (DMEM) (Gibco, Carlsbad, CA). This medium was supplemented with 10% fetal bovine serum (FBS) (Hyclone, Minneapolis, MN), 1% penicillin/streptomycin, 0.25% gentamicin and 0.25% fungizone and is referred to as the "control medium". The osteogenic medium consisted of control medium supplemented with 100 nM dexamethasone, 0.05 mM ascorbic acid and 10 mM β-glycerophosphate [34,35]. At 90% confluence cells were harvested by rinsing with a 0.25% trypsin and 0.03% EDTA solution and incubated at 37 °C until the cells detached.

Alginate was used as an encapsulating gel to protect the cells during the CPC setting reaction. Alginate is biocompatible and can form a cross-linked gel under mild conditions. A 1.2 wt.% sodium alginate solution was prepared by dissolving 0.3 g alginate (UP LVG, 64% guluronic acid, MW ≈ 75,000–220,000 g mol^{-1}, Pro-Nova Biomedical, Oslo, Norway) in 25 ml of 155 mM sodium chloride. Cells were encapsulated in alginate at a density of 1×10^6 cells ml^{-1} alginate solution. Bead formation was accomplished by extruding alginate/cell droplets through a sterile syringe fitted with a 25 gauge needle into individual wells of a 12-well cell culture plate containing 3 ml of 100 mmol l^{-1} calcium chloride solution to facilitate crosslinking. An aliquot of 1 ml of the cell/alginate suspension created approximately 114 beads. Therefore, the volume of alginate required to produce each bead was approximately 8.8 μl. The bead diameter (mean ± SD, $n = 10$) was measured using an optical stereomicroscope (Leica MZ16, Wetzlar, Germany) and calculated to be 2.2 ± 0.1 mm. The volume of the cross-linked bead was therefore reduced during gel formation to approximately 5.6 μl. This is a well-known phenomenon, whereby alginate droplets will shrink and lose water during gel formation after contact with calcium ions, resulting in an increase in the observed alginate and cell concentration in the cross-linked bead [36,37].

2.3. hBMSC–alginate–CPC construct preparation

Three types of CPC specimens were prepared: (1) CPC control, with sterile water as the CPC liquid; (2) CPC–chitosan, with 15% chitosan as the CPC liquid; (3) CPC–chitosan–fiber with 15% chitosan as the CPC liquid and 20% by volume Vicryl fibers for reinforcement.

Fifteen alginate beads containing hBMSCs at a concentration of approximately 8700 cells per bead were placed at the bottom of each well of a 12-well cell culture plate. Hence, each sample contained approximately 130,000 cells. Approximately 0.5 g of CPC paste was placed on top of the alginate beads. The volume of beads/(volume of CPC + volume of beads) was approximately 50%. The purpose of placing the beads in a cluster at the bottom and then covering them with the flowable CPC paste was to make it easier to collect the beads and cells later for analysis of live/dead cells and osteogenic differentiation. The CPC setting reaction is not exothermic and does not significantly increase the temperature of the beads. The cell–alginate–CPC constructs were allowed to set at 37 °C for 30 min. Then, fresh control medium was added to each well until the construct was completely submerged.

2.4. Mechanical testing

The CPC composite paste with cell-containing hydrogel beads was placed in a rectangular mold of 3 × 4 × 25 mm. Each specimen was set in a humidor for 4 h at 37 °C. The hardened specimen was removed from the molds and immersed in culture medium for 1 day. A three point flexural test was used to fracture the specimens in a Universal Testing Machine [32]. Flexural strength $S = 3F_{max}L/(2bh^2)$, where F_{max} is the maximum load on the load–displacement ($F-d$) curve, L is the span, b is the specimen width and h is the thickness. The elastic modulus $E = (F/d)(L^3/[4bh^3])$, where load F divided by displacement d is the slope. Work of fracture (toughness) (WOF) was calculated as the area under the $F-d$ curve divided by the specimen's cross-sectional area [38].

2.5. Live/dead assay

A live/dead assay was performed on days 1, 7, 14 and 21. The cell culture medium was removed and the hBMSC–alginate beads were removed from the CPC and washed with Dulbecco's phosphate-buffered saline, pH 7.2 (PBS). 2.0 ml of medium (without serum) containing 0.002 mmol l^{-1} calcein-AM and 0.002 mmol l^{-1} ethidium homodimer-1 (both from Invitrogen, Carslbad, CA) was added to each specimen. The cells were then observed by epifluorescence microscopy (Nikon Eclipse TE-2000S, Melville, NY). Live cells stained green, dead cells red.

Two parameters were measured. First, the percentage of live cells was measured, which was defined as $P_{Live} = N_{Live}/(N_{Live} + N_{Dead})$, where N_{Live} is the number of live cells and N_{Dead} is the number of dead cells in the same image. Six specimens of each material were tested ($n = 6$). Two randomly chosen fields of view were photographed for each specimen for a total of 12 photos per material.

The second parameter was live cell density D. This was measured as the percentage of specimen area that was covered by live cells. The cell density was measured as $D = (A_{calcein}/A_{Total})$, where $A_{calcein}$ is the area covered by live cells that stained green with calcein and A_{Total} was the total area of the field of view of the image.

2.6. Wst-1 cell viability assay

The Wst-1 assay is a colorimetric assay where the absorbance at 450 nm is proportional to the amount of dehydrogenase activity in the cells [39]. Higher absorbance values indicate increased production of the formazan product, which is correlated with cell viability. 2-(4-

Iodophenyl)-3-(4-nitrophenyl)-5-(2,4-disulfophenyl)-2H-tetrazolium, monosodium salt (Wst-1) and 1-methoxy-5-methylphenazinium methylsulfate (1-methoxy PMS) were obtained from Dojindo (Gaithersburg, MD). At each time point (1, 7, 14 and 21 days) the hBMSC–alginate beads from each specimen were recovered and washed with 1 ml of Tyrode's Hepes buffer. 1 ml of Tyrode's Hepes buffer and 100 ml of Wst-1 solution (5 mmol l^{-1} Wst-1 and 0.2 mmol l^{-1} 1-methoxy PMS in water) were then added to each well. After 4 h incubation at 37 °C, a 0.2 ml aliquot from each well was placed in a 96-well plate and the absorbance was measured with a microplate reader (Spectra-Max M5, Molecular Devices, Sunnyvale, CA).

2.7. Alkaline phosphatase activity

ALP is an enzyme expressed by cells during osteogenesis and has been shown to be a well-defined marker for their differentiation [40]. A colorimetric *p*-nitrophenyl phosphate assay (Stanbio, Boerne, TX) was used to measure ALP expression by the hBMSCs encapsulated in the CPC constructs. At each time point hBMSC–alginate beads were harvested and washed with PBS. 0.5 ml of sodium citrate buffer (55 mM sodium citrate, 0.15 M NaCl and 20 mM EDTA, pH 7.4) was added to each sample and incubated at 37 °C for 7 min to dissolve the alginate. Cells were collected by centrifugation and lysed with 0.5 ml of M-PER Mammalian Protein Extraction Reagent (Thermo Scientific, Rockford, IL). Lysates were assayed for ALP activity according to the manufacturer's protocol. Normal Control Serum (Stanbio), which contains a known concentration of ALP, was used as a standard. ALP activity was normalized to DNA concentration for each sample using the PicoGreen assay (Invitrogen, Carlsbad, CA) [41].

2.8. Mineral characterization

Mineral formation was investigated on days 7, 14 and 21, since previous studies found a large increase in calcium content in in vitro cell cultures from 12 to 21 days [42]. Xylenol orange, a fluorescent probe that chelates to calcium and stains mineral red was used for these experiments, because xylenol orange is not harmful to cells and, therefore, staining can be performed on live cells [42]. Xylenol orange (Sigma Aldrich, St. Louis, MO) was dissolved in water to make a 5 mM solution, which was subsequently sterile filtered.

At each time point the hBMSC–alginate beads were removed and washed with PBS. 2 ml of 20 mM xylenol orange was added and samples were incubated overnight. Prior to fluorescence imaging, the medium containing the respective fluorophores was removed and replaced with regular medium to prevent nonspecific background fluorescence. Both phase contrast and fluorescence images were collected for each sample. Mineral area A_{Mineral} was defined as $A_{\text{Mineral}} = (A_{\text{Fluorescence}}/A_{\text{Total}})$, where $A_{\text{Fluorescence}}$ is the area of stained mineralization and A_{Total} is the total area of the field of view of the image.

Scanning electron microscopy (SEM) (JEOL 5300, Peabody, MA) was used to examine the samples. The cell-encapsulating alginate beads were rinsed with 2 ml of PBS and fixed with 1% glutaraldehyde overnight. Samples were then subjected to graded alcohol dehydration, sputter coated with gold and viewed by SEM. Mineral deposition by the cells was also examined by X-ray diffraction (XRD). Alginate beads were pulverized between glass slides and then dried. The dried powder was collected and then compared with hydroxyapatite formed after the CPC had set. XRD patterns were recorded with a powder X-ray diffractometer (Rigaku, Danvers, MA) with graphite monochromatized CuKα radiation (λ = 0.154 nm) generated at 40 kV and 40 mA. All data were collected in continuous scan mode (1° 2θ min^{-1}, step time 0.6 s, step size 0.01°) and stored in a computer.

One-way and two-way ANOVA were performed to detect significant ($\alpha = 0.05$) effects of the variables. Tukey's multiple comparison procedures were used to compare the data at a family confidence coefficient of 0.95.

3. Results

3.1. Mechanical properties

Flexural strength, elastic modulus and WOF data for the CPC constructs are summarized in Table 1. The CPC–chitosan–fiber constructs exhibited a 5-fold increase in flexural strength compared with the CPC control, from 2.3 ± 0.94 to 11.7 ± 2.1 MPa, and an almost 4-fold increase in elastic modulus compared with the CPC control, from 0.53 ± 0.21 to 2.01 ± 0.39 GPa. Meanwhile, reinforcement by the addition of 20% fibers significantly increased the WOF to 1.65 ± 0.66 kJ m^{-2}, compared with the CPC control at 0.009 ± 0.005 kJ m^{-2} and CPC–chitosan at 0.015 ± 0.007 kJ m^{-2} ($P < 0.05$).

3.2. Cell viability

hBMSCs encapsulated in alginate and mixed with CPC-based pastes exhibited excellent viability (Fig. 1). Quantitatively, Fig. 2A indicates little difference in the percentage of live cells between cells encapsulated in alginate, in the CPC control, in the CPC–chitosan and in the CPC–chitosan–fiber constructs ($P > 0.05$). In Fig. 2B the live cell density significantly decreased from approximately 120 cells mm^{-2} on day 1 to 80 cells mm^{-2} on day 7 for all constructs ($P < 0.05$). The apparent decrease in live cell density after 1 day was the result of continued swelling of the alginate beads during cell culture. When freshly cross-linked alginate beads are placed in solution swelling occurs until equilibrium is reached. In our experiment cells were encapsulated in alginate and immediately mixed with the CPC paste. This served to delay swelling to the larger equilibrium volume until after 1 day. Since the bead volume on day 1 was smaller than at subsequent time points the apparent live cell density was greater on day 1 compared with later time points. After 7 days there was little change in the live cell density as a function of time ($P > 0.05$). Therefore, at each time point encapsulation in CPC constructs did not compromise hBMSC viability compared with those in alginate without CPC.

Cell viability was assessed using a Wst-1 assay (Fig. 3). On days 1, 7 and 14 the normalized absorbance for hBMSCs in alginate was 1.0 ± 0.04, significantly higher than that of the CPC control, the CPC–chitosan and the CPC–chitosan–fiber ($P < 0.05$). However, the CPC control, the CPC–chitosan and the CPC–chitosan–fiber constructs exhibited similar absorption values at all time points. This demonstrates that the addition of chitosan and fibers to CPC did not adversely affect viability when compared with the CPC control, which contained no chitosan or fibers.

3.3. ALP activity

Fig. 4 shows the ALP activity of hBMSCs in various constructs. ALP activity in osteogenic medium reached a maximum on day 14 for all constructs, with hBMSCs in alginate alone having the largest value (14.7 ± 4.1), which was significantly greater than the ALP activity of hBMSC–alginate–CPC constructs ($P < 0.05$). While this indicates greater osteogenic differentiation of hBMSCs in alginate alone, the significant increase in ALP activity of all hBMSC–CPC constructs on day 14 demonstrate that osteogenic differentiation was not affected by the reinforcing chitosan and fibers in CPC. In contrast, alginate beads alone and the CPC–chitosan–fiber cultured in control medium did not show any significant ALP activity during the course of the experiment ($P < 0.05$).

3.4. Mineralization via encapsulated hBMSCs

Mineralization by the encapsulated hBMSCs on days 7, 14 and 21 was visualized by staining with xylenol orange (Fig. 5A and B). Deposited mineral ranged between 20 and 50 μm in diameter. To quantify mineralization, the fractional area of mineral for each image was computed using NIS Elements imaging software (Nikon, Melville, NY) (Fig. 5C). On day 7 the amount of mineralization of hBMSCs in beads alone (1.4 ± 0.5%) was very similar to that of the CPC control (0.8 ± 0.3%), the CPC–chitosan (1.2 ± 0.4%) and the CPC–chitosan–fiber (0.7 ± 0.3%) ($P > 0.05$). On day 21 mineralization exhibited a 4-fold increase for most constructs compared with day 7, with hBMSCs in beads alone increasing to 5.0 ± 0.7%, compared with 3.6 ± 0.7% for the CPC control, 4.1 ± 0.9% for the CPC–chitosan and 4.5 ± 0.9% for the CPC–chitosan–fiber.

The SEM images in Fig. 6 illustrate the presence of mineral in the alginate beads after fixation and dehydration. Powder XRD analysis is presented in Fig. 7, where the peaks at 26° and 32° confirm the presence of apatitic mineral in the material harvested from alginate beads in the CPC–chitosan–fiber (Fig. 7A). These peaks were similar to those of known hydroxyapatite (Fig. 7B). Lower crystallinity is indicated by broader peaks at 26° and 32°.

4. Discussion

The present study investigated the viability and osteodifferentiation of hBMSCs when encapsulated in injectable and osteoconductive CPC-based constructs. Cells were encapsulated into alginate beads and subsequently mixed with either (1) a CPC control, (2) CPC reinforced with chitosan or (3) CPC reinforced with chitosan plus degradable Vicryl fibers. The encapsulated cells in CPC–chitosan and CPC–chitosan–fiber showed viabilities greater than 70% on day 21, comparable with cells in alginate without CPC and cells in the FDA approved CPC control without chitosan or fibers. Additionally, the encapsulated hBMSCs underwent osteogenic differentiation, as shown by increased ALP activity and mineral deposition as confirmed by mineral staining, SEM and powder XRD.

To be successful in repairing bone in moderate stress-bearing applications, tissue engineering scaffolds should have physical and mechanical properties to match those of natural bone. For example, the bulk modulus of cancellous bone ranges from 50 to 100 MPa [43]. In contrast, the elastic modulus of alginate hydrogels was found to be 0.136 MPa [44]. The elastic modulus of the CPC–chitosan–fiber constructs containing 50% by volume of alginate beads in our current study was 2 GPa, and its flexural strength was approximately 10 MPa. This matched the flexural strength of sintered porous hydroxyapatite, which has a flexural strength of 2–11 MPa [45]. This also exceeded the strength of cancellous bone, which was reported to be 3.5 MPa. The strong CPC–chitosan and CPC–chitosan–fiber composites have the added advantage of being moldable and can set in situ, resulting in intimate adaptation to complex bone cavities without machining. Furthermore, CPC is resorbable, while sintered hydroxyapatite is relatively stable in vivo [46]. This resorption allows the CPC to be gradually replaced over time by new bone while maintaining mechanical and dimensional stability.

After 1 day of cell culture encapsulated hBMSCs were shown in both live/dead staining and Wst-1 biocompatibility studies to be viable in CPC reinforced with chitosan and CPC reinforced with chitosan and Vicryl fibers (Figs. 1–3). The viability in these reinforced CPC constructs was comparable with the CPC control. This trend continued during the entire course of the experiment up to the 21 day end point. This suggests that the mechanically strong CPC–chitosan and CPC–chitosan–fiber composites were not harmful to the hBMSCs and elicited a cell response similar to that of the FDA approved CPC control. Cells encapsulated in alginate alone had significantly greater viability compared with the CPC

constructs when measured using Wst-1, however, scaffolds made exclusively from the alginate hydrogel did not have strength and mechanical properties comparable with the CPC-based materials, necessary for bone tissue engineering in load-bearing applications.

Previous studies have indicated that calcium phosphate cement disks did not support cell attachment and growth in vitro unless the disks were sintered at 1100 °C to convert α-TCP to β-TCP and enhance crystallinity [31]. In another calcium phosphate cement residual TTCP particles were present in the set CPC cement [47]. TTCP is alkaline and soluble and may compromise the hBMSCs by altering the pH in the microenvironment. In a recent study the hBMSCs appeared to be more sensitive to CPC ion activity than other cell types [48]. For example, ALP activity was successfully measured for rat mesenchymal stem cells cultured on CPC in a previous study [41], but not for the human mesenchymal stem cells on CPC [48]. CPC has been shown in vivo to have excellent osteoconductivity and new bone formation [49,50], where the in vivo dynamic circulation may minimize the effects of CPC ion activity and local pH changes in CPC on the cells. By encapsulating the hBMSCs in alginate beads and incorporating them into CPC pastes we accomplished two goals: (1) encapsulation of the stem cells in alginate beads protected the stem cells, allowing them to maintain viability and the ability to undergo osteogenic differentiation and mineralization; (2) after CPC setting the alginate beads had the potential to dissolve and release the cells, while concomitantly creating macroporosity in the CPC construct to enhance bone regeneration. The alginate beads in the current study were nondegradable and were used to demonstrate the efficacy of protecting cells from the CPC setting reaction by alginate encapsulation. To create macroporosity alginates that will degrade in a controlled manner over a finite period of time should be used to create the encapsulating beads.

The ALP activity of cells in alginate in the CPC control, CPC–chitosan and CPC–chitosan–fiber scaffolds showed a significant increase from day 1 to day 14 (Fig. 4), indicating that osteodifferentiation occurred, while hBMSCs in alginate in control medium exhibited minimal ALP activity throughout the experiment. Additionally, alginate beads in the CPC–chitosan–fiber constructs in control medium showed very little ALP activity up to day 14. Further evidence of osteogenic differentiation can be seen in Fig. 5, where mineral formation is shown at different time points and the amount of mineralization is plotted. A significant increase in mineral can qualitatively be seen for the CPC–chitosan–fiber composites from 7 to 21 days (Fig. 5A and B). Overall, hBMSCs encapsulated in alginate beads and mixed with the CPC control, CPC–chitosan and CPC–chitosan–fiber specimens exhibited a greater than 4-fold increase in mineral amount from day 7 to day 21. It may be expected that the calcium cross-linked alginate itself could give false positive staining using xylenol orange. However, previous studies showed that on day 1 alginate beads in the CPC–chitosan–fiber had a mineral coverage area of 0.09 ± 0.002%. If we assume that on day 1 the mineral content was exclusively from the alginate, it can be considered minimal and negligible compared with the cell-directed mineralization seen at later time points. SEM micrographs and powder XRD confirmed the presence of poorly crystalline apatite-like mineral, indicating that substantial osteogenic differentiation and mineralization occurred in the encapsulated hBMSCs.

5. Conclusion

The present study investigated hBMSC encapsulation in alginate hydrogel beads and in CPC control, in CPC–chitosan and in CPC–chitosan–fiber scaffolds. The percentage of live cells in the CPC–chitosan and CPC–chitosan–fiber scaffolds matched those on the FDA approved CPC control up to day 21. ALP activity of cells in the CPC control, the CPC–chitosan and the CPC–chitosan–fiber were all significantly higher than those in alginate alone in control medium. The ALP activity reached a maximum at 14 days, indicating osteogenic

differentiation. Furthermore, mineral staining with xylenol orange showed that mineral deposition by the hBMSCs occurred as early as 7 days and increased by 4-fold by day 21. SEM and powder XRD detected the presence of poorly crystalline hydroxyapatite-like mineral. Further studies should investigate hBMSC delivery in injectable CPC-based scaffolds by controlling the hydrogel bead size and degradation rate. In this manner the hydrogel beads can act as both a cell delivery system and a porogen for the higher mechanical strength CPC–chitosan scaffold. This new class of injectable, stem cell-encapsulating and mechanically strong scaffolds may find use in orthopedic and craniofacial applications, as well as minimally invasive surgery to enhance bone regeneration.

Acknowledgments

We thank Dr. Shozo Takagi, Dr. Lawrence Chow, Mr. Anthony Giuseppetti and Ms. Kathleen Hoffman of the American Dental Association Foundation for discussions and assistance with the SEM and powder X-ray diffraction analyses. We also thank Dr. Liang Zhao for assistance with the measurement of mechanical properties. This study was supported by NIH R01 Grants DE14190 and DE17974 (H.X.), a Maryland Nano-Biotechnology Award (H.X.), the Maryland Stem Cell Research Fund (H.X.) and the University of Maryland Dental School.

Appendix. Figures with essential color discrimination

Certain figures in this article, particularly Figures 1–5 and 7, are difficult to interpret in black and white. The full color images can be found in the on-line version, at doi:10.1016/j.actbio.2010.04.029.

References

1. Phillips JH, Forrest CR, Gruss JS. Current concepts in the use of bone grafts in facial fractures. Basic science considerations. Clin Plast Surg 1992;19:41–58. [PubMed: 1537227]
2. Salgado AJ, Coutinho OP, Reis RL. Bone tissue engineering: state of the art and future trends. Macromol Biosci 2004;4:743–765. [PubMed: 15468269]
3. Shanti RM, Li WJ, Nesti LJ, Wang X, Tuan RS. Adult mesenchymal stem cells: biological properties, characteristics, and applications in maxillofacial surgery. J Oral Maxillofac Surg 2007;65:1640–1647. [PubMed: 17656295]
4. Mao JJ. Stem cells and dentistry. J Dent Hyg 2009;83:173–174. [PubMed: 19909633]
5. Connelly JT, Garcia AJ, Levenston ME. Inhibition of in vitro chondrogenesis in RGD-modified three-dimensional alginate gels. Biomaterials 2007;28:1071–1083. [PubMed: 17123602]
6. Lawson MA, Barralet JE, Wang L, Shelton RM, Triffitt JT. Adhesion and growth of bone marrow stromal cells on modified alginate hydrogels. Tissue Eng 2004;10:1480–1491. [PubMed: 15588407]
7. Chung C, Burdick JA. Influence of three-dimensional hyaluronic acid microenvironments on mesenchymal stem cell chondrogenesis. Tissue Eng A 2009;15:243–254.
8. Keskar V, Marion NW, Mao JJ, Gemeinhart RA. In vitro evaluation of macroporous hydrogels to facilitate stem cell infiltration, growth, and mineralization. Tissue Eng A 2009;15:1695–1707.
9. Salinas CN, Anseth KS. Mesenchymal stem cells for craniofacial tissue regeneration: designing hydrogel delivery vehicles. J Dent Res 2009;88:681–692. [PubMed: 19734453]
10. Benoit DS, Schwartz MP, Durney AR, Anseth KS. Small functional groups for controlled differentiation of hydrogel-encapsulated human mesenchymal stem cells. Nat Mater 2008;7:816–823. [PubMed: 18724374]
11. Khan Y, Yaszemski MJ, Mikos AG, Laurencin CT. Tissue engineering of bone: material and matrix considerations. J Bone Joint Surg Am 2008;90 Suppl. 1:36–42. [PubMed: 18292355]
12. Franco J, Hunger P, Launey ME, Tomsia AP, Saiz E. Direct write assembly of calcium phosphate scaffolds using a water-based hydrogel. Acta Biomater 2009;6:218–228. [PubMed: 19563923]
13. Miranda P, Pajares A, Saiz E, Tomsia AP, Guiberteau F. Mechanical properties of calcium phosphate scaffolds fabricated by robocasting. J Biomed Mater Res A 2008;85:218–227. [PubMed: 17688280]

14. Kasten P, Beyen I, Niemeyer P, Luginbuhl R, Bohner M, Richter W. Porosity and pore size of beta-tricalcium phosphate scaffold can influence protein production and osteogenic differentiation of human mesenchymal stem cells: an in vitro and in vivo study. Acta Biomater 2008;4:1904–1915. [PubMed: 18571999]
15. Montufar EB, Traykova T, Gil C, Harr I, Almirall A, Aguirre A, et al. Foamed surfactant solution as a template for self-setting injectable hydroxyapatite scaffolds for bone regeneration. Acta Biomater 2010;6:876–885. [PubMed: 19835998]
16. Hing KA, Best SM, Bonfield W. Characterization of porous hydroxyapatite. J Mater Sci Mater Med 1999;10:135–145. [PubMed: 15348161]
17. Hench LL. Bioceramics. J Am Ceram Soc 1998;81:1705–1728.
18. Deville S, Saiz E, Tomsia AP. Freeze casting of hydroxyapatite scaffolds for bone tissue engineering. Biomaterials 2006;27:5480–5489. [PubMed: 16857254]
19. LeGeros RZ. Biodegradation and bioresorption of calcium phosphate ceramics. Clin Mater 1993;14:65–88. [PubMed: 10171998]
20. Barralet JE, Gaunt T, Wright AJ, Gibson IR, Knowles JC. Effect of porosity reduction by compaction on compressive strength and microstructure of calcium phosphate cement. J Biomed Mater Res 2002;63:1–9. [PubMed: 11787022]
21. Chow LC, Takagi S, Costantino PD, Friedman CD. Self-setting calcium phosphate cements. Mater Res Soc Symp Proc 1991;179:3–24.
22. Brown, WE.; Chow, LC. A new calcium phosphate water setting cement. In: Brown, PW., editor. Cements research progress. Westerville, OH: American Ceramic Society; 1986. p. 352-379.
23. Espanol M, Perez RA, Montufar EB, Marichal C, Sacco A, Ginebra MP. Intrinsic porosity of calcium phosphate cements and its significance for drug delivery and tissue engineering applications. Acta Biomater 2009;5:2752–2762. [PubMed: 19357005]
24. Ginebra MP, Traykova T, Planell JA. Calcium phosphate cements as bone drug delivery systems: a review. J Control Release 2006;113:102–110. [PubMed: 16740332]
25. Bohner M, Baroud G. Injectability of calcium phosphate pastes. Biomaterials 2005;26:1553–1563. [PubMed: 15522757]
26. Habib M, Baroud G, Gitzhofer F, Bohner M. Mechanisms underlying the limited injectability of hydraulic calcium phosphate paste. Acta Biomater 2008;4:1465–1471. [PubMed: 18445539]
27. Friedman CD, Costantino PD, Takagi S, Chow LC. BoneSource hydroxyapatite cement: a novel biomaterial for craniofacial skeletal tissue engineering and reconstruction. J Biomed Mater Res 1998;43:428–432. [PubMed: 9855201]
28. Bifano CA, Edgin WA, Colleton C, Bifano SL, Constantino PD. Preliminary evaluation of hydroxyapatite cement as an augmentation device in the edentulous atrophic canine mandible. Oral Surg Oral Med Oral Pathol Oral Radiol Endod 1998;85:512–516. [PubMed: 9619665]
29. Xu HH, Quinn JB, Takagi S, Chow LC. Synergistic reinforcement of in situ hardening calcium phosphate composite scaffold for bone tissue engineering. Biomaterials 2004;25:1029–1037. [PubMed: 14615168]
30. Weir MD, Xu HH, Simon CG Jr. Strong calcium phosphate cement-chitosan-mesh construct containing cell-encapsulating hydrogel beads for bone tissue engineering. J Biomed Mater Res A 2006;77:487–496. [PubMed: 16482548]
31. Link DP, van den DJ, Wolke JG, Jansen JA. The cytocompatibility and early osteogenic characteristics of an injectable calcium phosphate cement. Tissue Eng 2007;13:493–500. [PubMed: 17362133]
32. Xu HH, Quinn JB, Takagi S, Chow LC, Eichmiller FC. Strong and macroporous calcium phosphate cement: effects of porosity and fiber reinforcement on mechanical properties. J Biomed Mater Res 2001;57:457–466. [PubMed: 11523041]
33. Xu HH, Simon CG Jr. Self-hardening calcium phosphate composite scaffold for bone tissue engineering. J Orthop Res 2004;22:535–543. [PubMed: 15099632]
34. Bruder SP, Jaiswal N, Haynesworth SE. Growth kinetics, self-renewal, and the osteogenic potential of purified human mesenchymal stem cells during extensive subcultivation and following cryopreservation. J Cell Biochem 1997;64:278–294. [PubMed: 9027588]

35. Nuttelman CR, Tripodi MC, Anseth KS. In vitro osteogenic differentiation of human mesenchymal stem cells photoencapsulated in PEG hydrogels. J Biomed Mater Res A 2004;68:773–782. [PubMed: 14986332]
36. De Vos P, De Haan B, Wolters GHJ, Van Schilfgaarde R. Factors influencing the adequacy of microencapsulation of rat pancreatic islets. Transplantation 1996;62:888–893. [PubMed: 8878379]
37. Orive G, Hernandez RM, Gascon AR, Igartua M, Pedraz JL. Survival of different cell lines in alginate-agarose microcapsules. Eur J Pharm Sci 2003;18:23–30. [PubMed: 12554069]
38. Xu HH, Quinn JB. Calcium phosphate cement containing resorbable fibers for short-term reinforcement and macroporosity. Biomaterials 2002;23:193–202. [PubMed: 11763861]
39. Ishiyama M, Tominaga H, Shiga M, Sasamoto K, Ohkura Y, Ueno K. A combined assay of cell viability and in vitro cytotoxicity with a highly water-soluble tetrazolium salt, neutral red and crystal violet. Biol Pharm Bull 1996;19:1518–1520. [PubMed: 8951178]
40. Wang J, de Boer J, de Groot K. Proliferation and differentiation of MC3T3-E1 cells on calcium phosphate/chitosan coatings. J Dent Res 2008;87:650–654. [PubMed: 18573985]
41. Moreau JL, Xu HH. Mesenchymal stem cell proliferation and differentiation on an injectable calcium phosphate-chitosan composite scaffold. Biomaterials 2009;30:2675–2682. [PubMed: 19187958]
42. Wang YH, Liu Y, Maye P, Rowe DW. Examination of mineralized nodule formation in living osteoblastic cultures using fluorescent dyes. Biotechnol Prog 2006;22:1697–1701. [PubMed: 17137320]
43. Gibson LJ. The mechanical-behavior of cancellous bone. J Biomechanics 1985;18:317–328.
44. Kong HJ, Kaigler D, Kim K, Mooney DJ. Controlling rigidity and degradation of alginate hydrogels via molecular weight distribution. Biomacromolecules 2004;5:1720–1727. [PubMed: 15360280]
45. Suchanek W, Yoshimura M. Processing and properties of hydroxyapatite-based biomaterials for use as hard tissue replacement implants. J Materials Res 1998;13:94–117.
46. Garrett S. Periodontal regeneration around natural teeth. Ann Periodontol 1996;1:621–666. [PubMed: 9118274]
47. Burguera EF, Xu HHK, Takagi S, Chow LC. High early strength calcium phosphate bone cement: effects of dicalcium phosphate dihydrate and absorbable fibers. J Biomed Mater Res A 2005;75A: 966–975. [PubMed: 16123976]
48. Weir MD, Xu HH. Culture human mesenchymal stem cells with calcium phosphate cement scaffolds for bone repair. J Biomed Mater Res B Appl Biomater 2010;93:93–105. [PubMed: 20091907]
49. Fujikawa K, Sugawara A, Murai S, Nishiyama M, Takagi S, Chow LC. Histopathological reaction of calcium phosphate cement in periodontal bone defect. Dent Mater J 1995;14:45–57. [PubMed: 8940545]
50. Sugawara A, Fujikawa K, Kusama K, Nishiyama M, Murai S, Takagi S, et al. Histopathologic reaction of a calcium phosphate cement for alveolar ridge augmentation. J Biomed Mater Res 2002;61:47–52. [PubMed: 12001245]

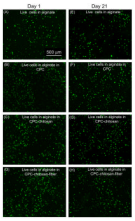

Fig. 1.
hBMSCs encapsulated in alginate on day 1: (A) live cells in alginate alone; (B) live cells in CPC control; (C) live cells in CPC–chitosan; (D) live cells in CPC–chitosan–fiber. hBMSCs encapsulated in alginate on day 21: (E) live cells in alginate alone; (F) live cells in CPC control; (G) live cells in CPC–chitosan; (H) live cells in CPC–chitosan–fiber.

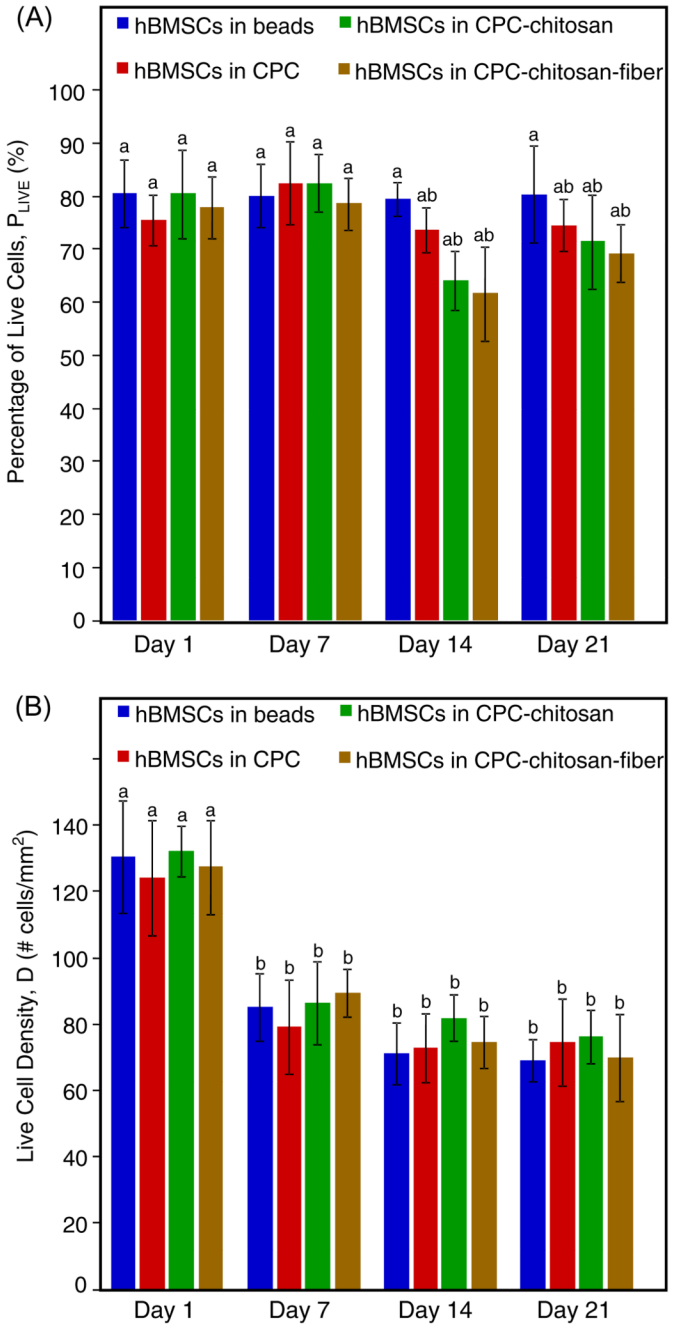

Fig. 2.

Live/dead results of encapsulated hBMSCs inside alginate hydrogel beads, CPC, CPC–chitosan and CPC–chitosan–fiber constructs (means ± SD, $n = 6$). (A) Percentage of live cells on days 1, 7, 14 and 21. (B) Live cell density inside the four different constructs on days 1, 7, 14 and 21. Dissimilar letters in the plot indicate values that are significantly different (Tukey's multiple comparison test, family confidence coefficient 0.95).

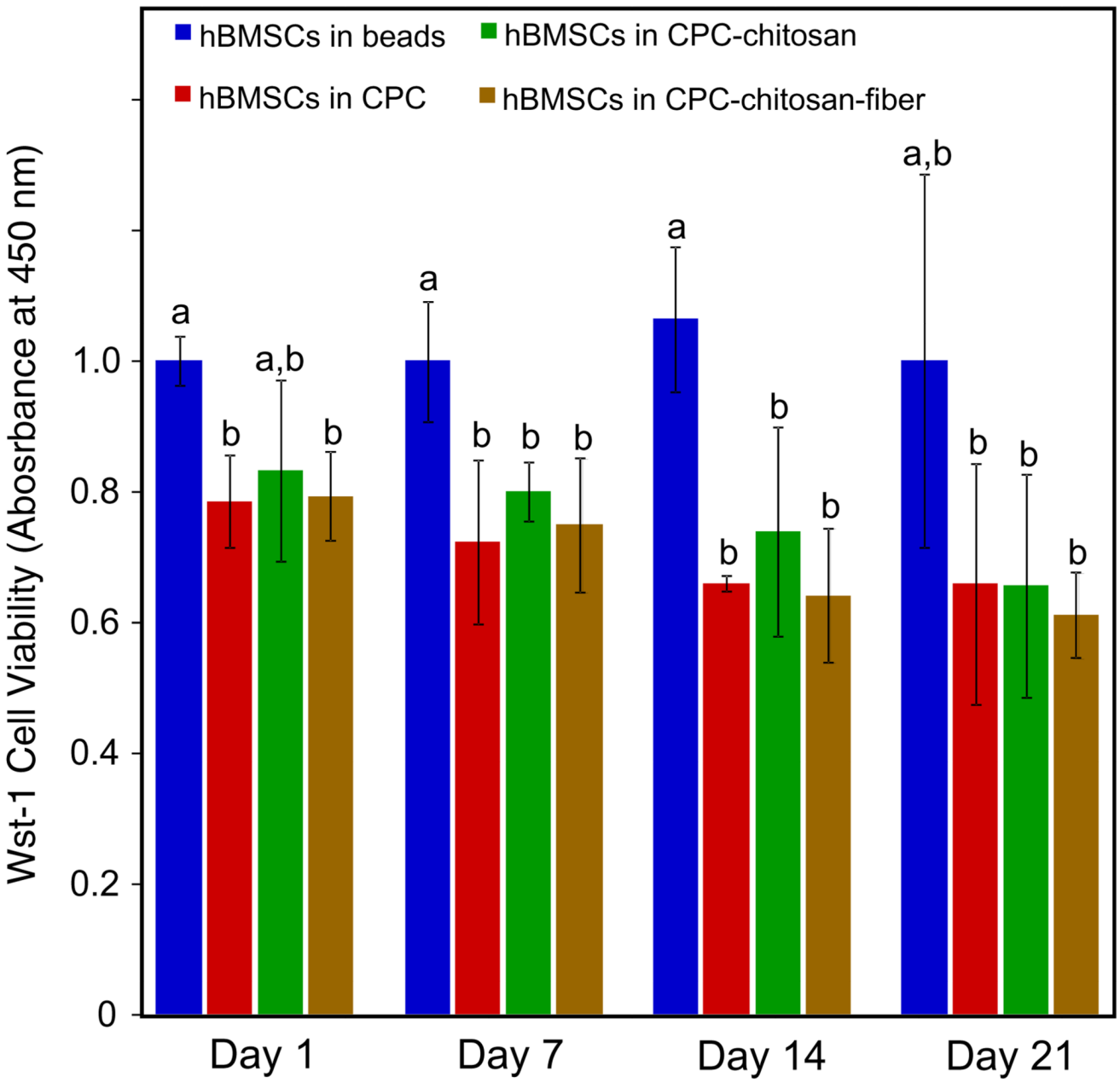

Fig. 3.

Wst-1 assay results for encapsulated hBMSCs inside alginate hydrogel beads, CPC, CPC–chitosan and CPC–chitosan–fiber constructs (means ± SD, $n = 6$). The viability of hBMSCs was quantified by recording the absorbance at 450 nm as an indication of dehydrogenase activity. Dissimilar letters in the plot indicate values that are significantly different (Tukey's multiple comparison test, family confidence coefficient 0.95).

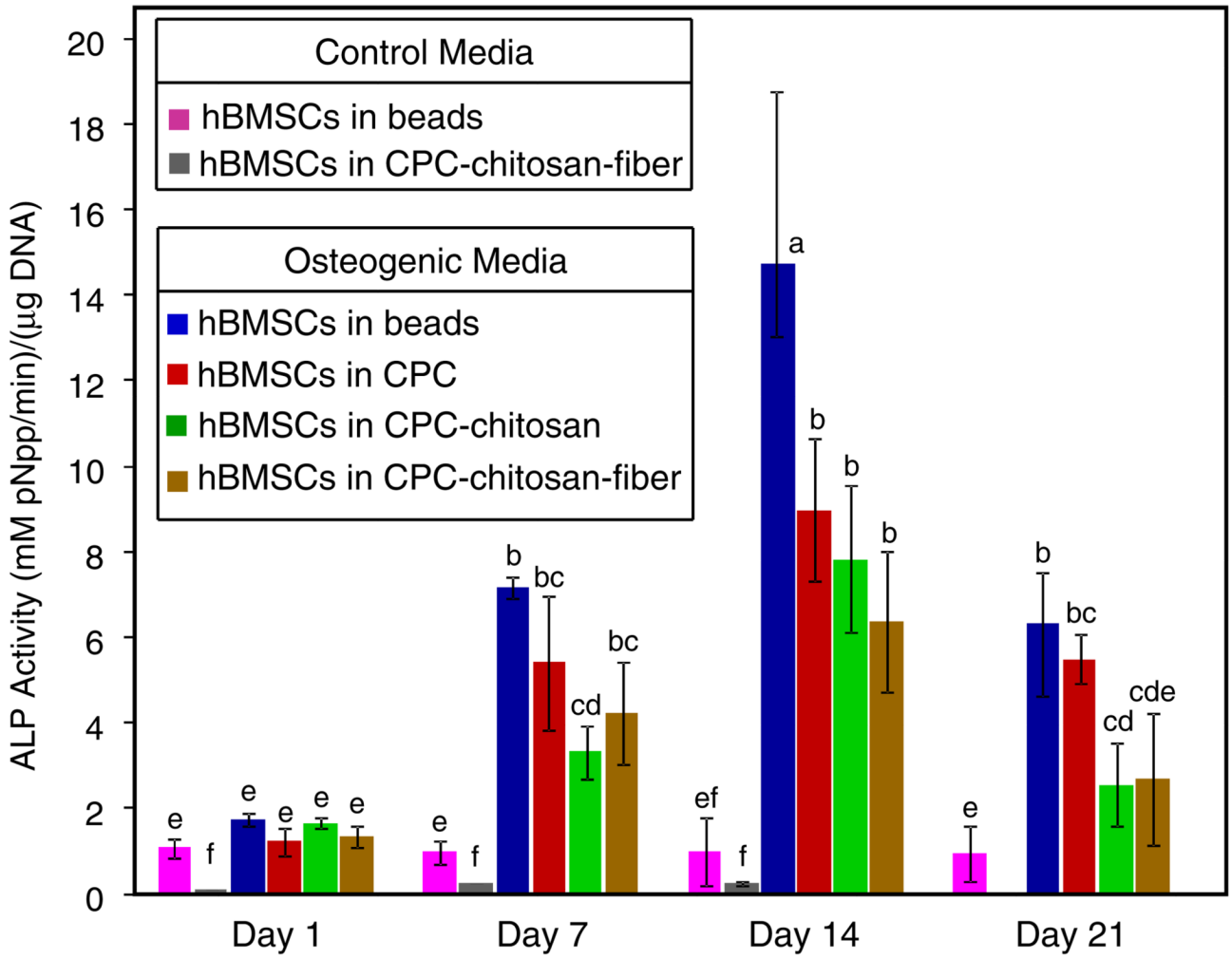

Fig. 4.

ALP activity of encapsulated hBMSCs inside alginate hydrogel beads, and inside CPC, CPC–chitosan and CPC–chitosan–fiber constructs (means ± SD, $n = 6$). The ALP value was normalized to the DNA concentration, with units of mM pNpp min^{-1}/µg DNA. Dissimilar letters in the plot indicate values that are significantly different (Tukey's multiple comparison test, family confidence coefficient 0.95).

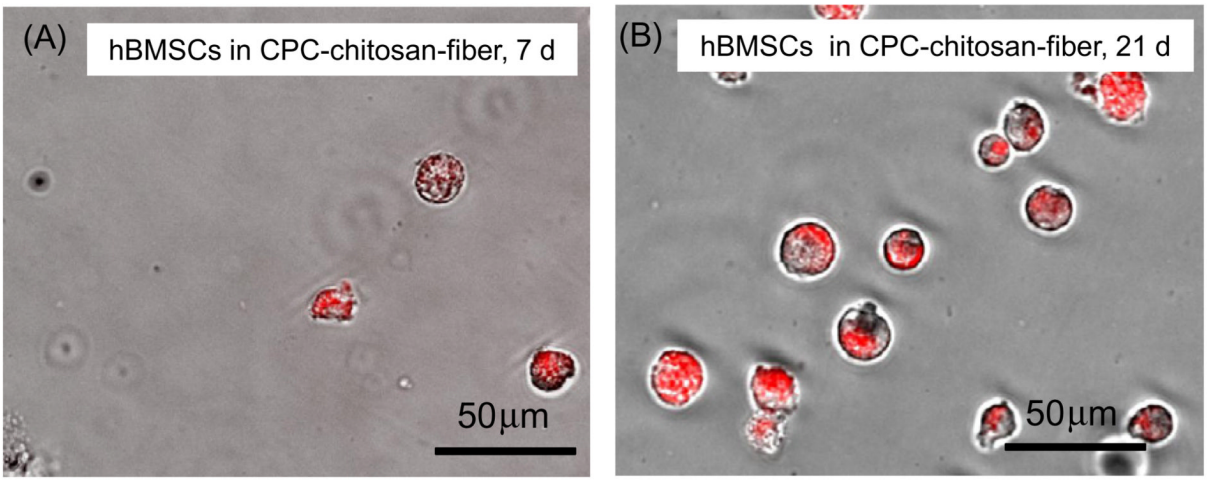

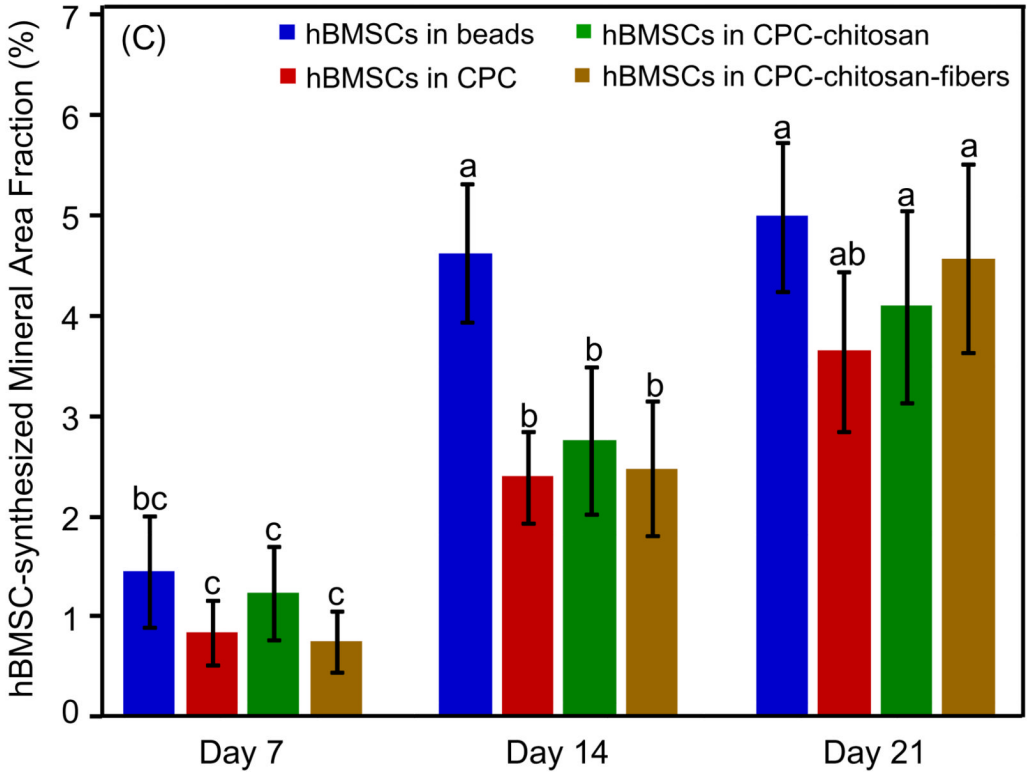

Fig. 5.

Mineralization by hBMSCs in hydrogel beads in the CPC–chitosan–fiber construct on (A) day 7 and (B) day 14, cultured in osteogenic medium. The live cell culture was stained with xylenol orange, which stains mineral a red color (means ± SD, $n = 6$). (C) hBMSC mineralization area fraction, which is the area of stained mineralization divided by the total area of the field of view of the image. This was done for the encapsulated hBMSCs in alginate hydrogel beads, in CPC, in CPC–chitosan and in CPC–chitosan–fiber constructs. Dissimilar letters in (C) indicate values that are significantly different (Tukey's multiple comparison test, family confidence coefficient 0.95).

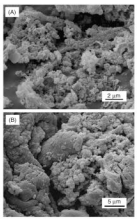

Fig. 6.
SEM showing significant mineral formation via hBMSCs. (A) Mineral synthesized by hBMSCs encapsulated in alginate hydrogel beads on day 21 and (B) mineral synthesized by hBMSCs encapsulated in beads in the CPC–chitosan–fiber construct on day 21.

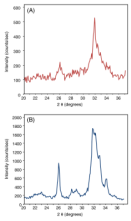

Fig. 7.
Powder XRD pattern of minerals. XRD patterns of (A) the hBMSC-synthesized minerals collected on day 21 from beads in the CPC–chitosan–fiber constructs and (B) a known hydroxyapatite, formed by calcium phosphate cement conversion and provided by Dr. Shozo Takagi of the National Institute of Standards and Technology.

Table 1

Mechanical properties of CPC constructs. Constructs contain 50% v/v alginate beads and 130,000 hBMSCs.

Material	Flexural strength (MPa)	Elastic modulus (GPa)	Work-of-fracture (kJ m^{-2})
CPC	2.3 ± 0.9	0.53 ± 0.21	0.009 ± 0.005
CPC–chitosan	3.5 ± 1.1	0.67 ± 0.18	0.015 ± 0.007
CPC–chitosan–fibers	11.7 ± 2.1	2.01 ± 0.39	1.66 ± 0.66